Solar Energy Materials & Solar Cells 251 (2023) 112116

Contents lists available at ScienceDirect

Solar Energy Materials and Solar Cells

journal homepage: www.elsevier.com/locate/solmat

Caesium doping accelerates the hydration rate of potassium carbonate in thermal energy storage

Jelle Houben [a], Aleksandr Shkatulov [a], Henk Huinink [a,b,*], Hartmut Fischer [c], Olaf Adan [a,c]

[a] Eindhoven University of Technology, Den Dolech 2, 5600 MB Eindhoven, The Netherlands
[b] EIRES, Horsten 1, 5612 AX Eindhoven, The Netherlands
[c] TNO Materials Solutions, High Tech Campus 25, 5656 AE Eindhoven, The Netherlands

ARTICLE INFO

Keywords:
Potassium carbonate
Thermochemical material
Doping
Caesium carbonate
Heat battery

ABSTRACT

Potassium carbonate has recently been identified as a promising candidate for thermochemical energy storage. However, as for many salt hydrates, its reaction kinetics is relatively slow. K_2CO_3 has a metastable zone, where the reaction is kinetically hindered, which limits the temperature operating window. This work aims to improve the material performance, focusing on two aspects; improving the kinetics outside the metastable zone and reducing the metastable zone width. This work shows that doping with Cs_2CO_3, can improve both. Moreover, it is shown that the dopant enhances the hydration rate by introducing mobility due to local deliquescence. This lays the foundation for further material research using dopants to enhance the performance of salt hydrates.

1. Introduction

In the Paris Agreement 2015 it is recognized that there is an urgent threat of climate change [1]. The agreement thereby quantifies the goal as the objective to hold: "the increase in the global average temperature to well below 2 °C above pre-industrial levels and to pursue efforts to limit the temperature increase to 1.5 °C above pre-industrial levels, recognizing that this would significantly reduce the risks and impacts of climate change" [2].

To meet this objective, a transition has to be made from a fossil fuel-based society to a renewable energy-based society. In this transition, the increase of renewable energies and the development of efficient energy systems are essential. To increase energy efficiency, the production of energy should be as close as possible to the end-user, thus decentralizing the energy system. Amongst these decentralized energy systems are; combined heat and power, district heating and cooling, geothermal, biomass and solar energy [3].

For decentralized systems, energy storage is a key component to match energy demand and energy supply in time and power. Storage is particularly crucial for thermal energy systems based on solar energy, which often offer their highest peak during periods of low demand i.e. high solar irradiation in summer and high heat demand in winter.

In the field of heat storage, a promising concept is based on thermochemical heat storage. In this concept, sorption energy is used to store heat in a reversible chemical reaction. Sorption is defined as the fixation of a gas or vapour (sorbate) by a solid or liquid (sorbent) [4]. A promising subclass of thermochemical materials (TCM's) are salt hydrates, as they feature a high energy density, a hydration/dehydration temperature suitable for domestic applications and a safe sorbate (i.e. water vapour) [5].

Salt hydrates incorporate water in the crystal lattice, the hydration reaction is exothermic and the output temperature is dependent on the water vapour pressure. Donkers et al. [6] made an extensive analysis of salt hydrates including 563 hydration reactions, from which K_2CO_3 was selected as the most promising material, based on the temperature operating window, stability, price and safety. In this analysis, the focus was on domestic heat storage.

The gas–solid equilibrium reaction of K_2CO_3 is given by:

$$K_2CO_3(s) + 1.5H_2O(g) \Longleftrightarrow K_2CO_3 \cdot 1.5H_2O(s), \quad (1)$$

wherein the hydration reaction from left to right is exothermic and energy is released when water is absorbed. The dehydration reaction from right to left is endothermic and heat is stored by desorption of water.

For domestic heat storage, it is of crucial importance to match hydration and dehydration temperatures to the required temperature window. To match these temperatures, phase diagrams are used. Fig. 1 shows the phase diagram of K_2CO_3 [7–10]. On the Y-axis the water vapour pressure is plotted against temperature on the X-axis. The solid green line above the dashed grey area is the K_2CO_3 equilibrium phase line as found by Glasser [7]. Above the equilibrium line, the hydrate ($K_2CO_3 \cdot 1.5\ H_2O$) is thermodynamically stable and below the equilibrium line the anhydrate (K_2CO_3) is stable.

* Corresponding author at: Eindhoven University of Technology, Den Dolech 2, 5600 MB Eindhoven, The Netherlands.
E-mail address: h.p.huinink@tue.nl (H. Huinink).

https://doi.org/10.1016/j.solmat.2022.112116
Received 4 April 2022; Received in revised form 24 October 2022; Accepted 16 November 2022
Available online 6 December 2022

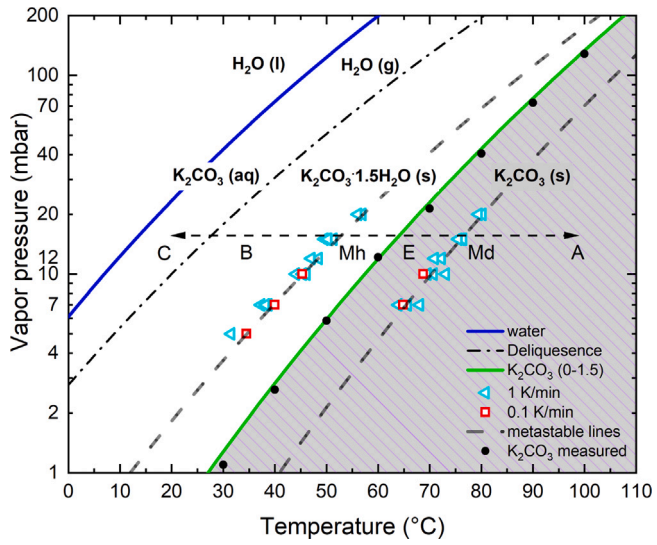

Fig. 1. Phase diagram of K_2CO_3 indicating the equilibrium line (solid line with measured points in dots), the metastable zone (MSZ) indicated by the dashed lines wherein the upper dashed line refers to hydration and the lower to dehydration. The dashed–dotted line is the deliquescence line and the blue line is the water equilibrium line. Dots are the measured equilibrium points [11], Figure adapted from Sögütoglu et al. [12]. The capital letters refer to a measurement sequence and will be explained in method Section 2.4.

For a heat storage application, the equilibrium behaviour is needed to understand the temperature window in which the salt will hydrate or dehydrate. But as important is the kinetics of the material, reflecting how fast a system can be charged or discharged, thus the power the material can deliver on system level. A kinetic study of Sögütoglu et al. [12] shows that, close to equilibrium conditions, hydration is kinetically hindered and a hydration/dehydration reaction is only observed after an induction period. This behaviour is called metastable behaviour and is caused by a free energy barrier for nucleation, where surface energy has to be overcome to make a transition from a local minimum in free energy to a global minimum [13]. From this work, it is concluded that the phase transition is mediated by a local dissolution at the interface [14]. Due to this metastable behaviour, the temperature operating window is reduced, since the maximum hydration temperature is not determined by the equilibrium line but by the metastable line for hydration. The same holds for the minimum dehydration temperature. Metastable behaviour is found for several other salts; $CuCl_2$, $MgSO_4$, $ZnSO_4$ and Na_2SO_4 [12,15–17].

Currently, a disadvantage of salt hydrates is that they exhibit relatively slow kinetics [18], especially compared to adsorption materials like zeolites or silica gel [19]. To improve kinetics and, additionally, overcome metastable behaviour, doping can be used to enhance material performance. Doping is performed by the introduction of small amounts of alien ions to the base material to promote nucleation and thereby improve kinetics of the base material. The potential effect of doping is successfully demonstrated by Shkatulov et al. [20]. They showed that, by doping $Mg(OH)_2$ with $NaNO_3$, the decomposition temperature could be lowered. This was also shown by doping $Mg(OH)_2$ and $Ca(OH)_2$ with several chlorides, nitrates, acetates and sulphates [21]. Moreover kinetic improvements are found by doping of $Ca(OH)_2$ with KNO_3 [22].

Dopants can be introduced in the bulk or on the surface of the crystal of K_2CO_3, resulting in several possible mechanisms affecting the hydration reaction e.g.: heterogeneous nucleation by lowering the interfacial energy, changing the crystal stability, improving the surface mobility or affecting the deliquescence relative humidity (DRH).

The aim of this study is to understand the basic mechanism underpinning doping effects on phase transitions and to find possible doping candidates that improve the hydration behaviour of K_2CO_3 in two ways; first to increase the temperature operating window by reducing the metastable zone width (MZW) and secondly to improve the kinetics, both in- and outside the metastable zone (MSZ). Possible doping candidates are selected based on three selection criteria: cation substitution, mono-valency and solubility. From these criteria the group 1 elements: Li_2CO_3, Na_2CO_3, Rb_2CO_3 and Cs_2CO_3 were selected. These candidates were then screened based on both the effect on the MZW and kinetics. Finally, it is investigated how the dopant is incorporated into the base material and which mechanism is underlying the observed doping effects.

2. Materials and methods

2.1. Dopant selection

Doping candidates are selected based on three criteria: cation doping, mono-valency and solubility.

The first candidates are selected based on cation doping. In potassium carbonate the cation is mono-atomic and the anion is poly-atomic. Due to this poly-atomic character it is less straightforward to understand the substitution behaviour, as charge distribution is more complex with its trigonal planar structure. Consequently this limits the candidates to carbonate salts.

Secondly we are selecting monovalent ions. For the doping to be stable, both during preparation and during cycling, the dopant should be compatible electrostatically, otherwise the ionic structure would have to change.

Finally, the dopants have to be soluble since the materials will be prepared with evaporative crystallization, as it is one of the most common and simplest crystallization methods. Therefore, the soluble carbonates of group 1 elements: Li_2CO_3, Na_2CO_3, Rb_2CO_3 and Cs_2CO_3 are selected, $SrCO_3$ and $BaCO_3$ are not used since they are insoluble. The solubilities for Li_2CO_3, Na_2CO_3, K_2CO_3, Rb_2CO_3 and Cs_2CO_3 are; 13, 164, 1105, 4500 and 2600 g/l respectively.

2.2. Sample preparation

All samples, including pure potassium carbonate, are prepared via the same method; forced crystallization using a rotary evaporator. Both Rb_2CO_3 and Cs_2CO_3 have a solubility higher than K_2CO_3 (4500 and 2600 g/l respectively) and are mixed at a mol ratio of 1:20. Li_2CO_3 and Na_2CO_3 are prepared in such a concentration that the volume of the saturated solution of both K_2CO_3 and dopant are equal. This is done since Li_2CO_3 and Na_2CO_3 have a solubility lower then K_2CO_3 (13 and 164 g/l respectively) they will crystallize earlier than K_2CO_3. Consequently, the increase in concentration during evaporation is proportional for both K_2CO_3 and Li_2CO_3 (or Na_2CO_3). Therefore, the point of crystallization onset for K_2CO_3 and dopant is closest as possible. In this way, segregated crystallization is prevented as much as possible. A slight deviation can occur, since the actual saturation point can deviate since the solubility data is based on single salt solubilities. In binary solutions the solubility can decrease due to the common ion effect of the carbonate salts. Furthermore, the Cs_2CO_3 doping content is varied in the ratios; 1, 2, 4, 6, 10-:100 (mol:mol), in order to evaluate how the doping content is affecting the behaviour of the material. In this work the onset point is defined as; the point where the reactions start (hydration, dehydration or deliquescence reaction). The onset point can be determined by scanning through the phase diagram, either by keeping the temperature constant and varying the water vapour pressure, or by fixing the vapour pressure and scanning through temperature. In this work the latter method is used.

All carbonate salts are first dissolved until the solution is saturated. Then the saturated solutions are filtered with a Millex®-GP syringe filter with a 0.22 μ m pore size to remove large seed crystals. After the seed crystals are removed the saturated solution of K_2CO_3 and

dopant are mixed. Due to a large difference in solubility (13–4500 g/l), separate crystallization of K_2CO_3 and dopant should be prevented, using a fast crystallization method by means of a rotary evaporator.

The filtered and mixed saturated solutions are prepared in the evaporating flask of a Buchi® Rotavapour R-200. The water bath temperature is set at a temperature of 80 °C with a low pressure conditioned at 60 mbar. During preparation the flask rotates and thereby creating a thin film in which the salt crystallizes quickly. After crystallization the powder is post-dried in an oven at 130 °C to remove the bound crystal water and $KHCO_3$ impurities. Finally, the dried material is grinded and sieved into a fraction between 50–160 μm.

To verify if observed changes on the behaviour of K_2CO_3 are caused by the dopant or the preparation method, two additional preparation methods are used for comparison, i.e. freeze drying and melting. For freeze drying, the preparation is similar to the rotary evaporator; the mixed saturated solutions are prepared in a rotating round flask, which is submerged in liquid nitrogen. After the solution is completely frozen as a thin film, the flask is connected to a vacuum pump and slowly all water is removed by sublimation during a period of at least 12 h. For the preparation via melt, the dry powders are manually grounded with a mortar. The powders are mixed in a mol ratio of 1:20 and the mixing is done using a vortex shaker. The mixed salts are then melted in a Lenton® AWF130/12 wire furnace at 950 °C in blank steel crucibles, while purging the oven with argon to prevent oxidation.

An overview with all prepared samples can be found in the following table, the doping content has been checked with ion chromatography (see Table 1).

Table 1
Overview of dopants, preparation methods and content, the first column represents the dopant concentration in molar ratio, the second in mass ratio.

Dopant	Preparation method	Content [mol x:100]	Content [mass x:100]
Li_2CO_3	Rotary evaporator	2.2	1.2
Na_2CO_3	Rotary evaporator	19.4	12.9
Rb_2CO_3	Rotary evaporator	5	8.4
Cs_2CO_3	Rotary evaporator	5	11.8
Cs_2CO_3	Rotary evaporator	1	2.4
Cs_2CO_3	Rotary evaporator	2	4.7
Cs_2CO_3	Rotary evaporator	4	9.4
Cs_2CO_3	Rotary evaporator	6	14.1
Cs_2CO_3	Rotary evaporator	10	23.6
Cs_2CO_3	Melting	5	11.8
Cs_2CO_3	Freeze drying	5	11.8

2.3. Selection method for dopants

In this section two methods are described which are used to screen the effects of the used dopants, effect on onset points and effect on kinetics. With onset point is meant is the starting point of a specific transition. Using TGA, the transition can be observed by a change in mass when we are varying the temperature at constant vapour pressure. A first screening of the dopants will be done on the effect of the doping on the temperature onset points. These are the onset points for the hydration, dehydration and deliquescence transition. This screening focuses on the effect of narrowing the metastable zone width rather than enhancing the kinetics outside the metastable zone. This is because the kinetics can be influenced by parameters as primary crystallite size, morphology, particle size and size distribution, which requires an comprehensive analysis. No effect on onset points this does not imply there is no effect on kinetics, the kinetic screening is the second screening method. To measure kinetics, a different type of measurement is performed, both will be elaborated in the following section.

2.4. Thermogravimetric analyses (TGA)

Both screening experiments are performed on a Mettler Toledo® TGA/DSC 3+ thermal analyser which has a balance with 1 g capacity, an accuracy of 1 μg and a temperature range from 20 till 1100 °C. Transition onset points are determined by changing the temperature at a constant rate at fixed water vapour pressure. Change in mass is then registered as the onset point. Water vapour is introduced via the purge gas supply at a flow rate of 300 ml/min. The water vapour pressure is controlled by mixing a wet gas (nitrogen at 100% RH) at 18 °C and a dry gas (nitrogen at 0% RH) at a desired ratio. The water vapour in the wet gas is supplied by an home-built build humidifier working with a Nafion™ semi-permeable membrane. The RH is defined through the temperature of liquid water. The RH in the measurement chamber of the TGA is calibrated using the deliquescence points of LiCl, CH_3CO_2K, $MgCl_2$, K_2CO_3 and $Mg(NO_3)_2$ at 25 °C [23].

For determining the onset points of hydration, dehydration and deliquescence, heating and cooling runs are performed at isobaric conditions (17 mbar), shown in Fig. 1. For the hydration onset measurement, the prepared material is fully anhydrous. The starting temperature, point A in Fig. 1, is far above the equilibrium temperature for pure potassium carbonate given the isobaric vapour condition. From point A on, the temperature is lowered with a cooling rate of 1 K/min towards point B. From the known equilibrium line, hydration is expected when the temperature reaches point E, but due to metastable behaviour of pure potassium carbonate hydration is observed at point Mh. For all dopants the effect on the hydration onset point Mh is determined.

For dehydration onset points, similar experiments are performed whereby, the starting material is fully hydrous and the measurement starts at point B. The temperature is increased with a heating rate of 1 K/min to find the metastable onset point for dehydration around point Md.

For the deliquescence onset point the material is prepared as completely hydrous. Starting from 40 °C at point B, the temperature is decreased with a cooling rate of 1 K/min towards point C.

Kinetic hydration experiments are performed under isothermal (40 °C) and isobaric (12 mbar) conditions. The material is in-situ dehydrated at 140 °C while purging with dry nitrogen. Then the material is thermally equilibrated for 1 h at 40 °C, after which the water vapour pressure is switched to 12 mbar and the hydration starts. The rate can then be determined by the time derivative of the water uptake.

2.5. XRD

To study the influence of the dopant on the crystal structure and the primary crystallite size, X-ray powder diffraction analysis is performed using a Rigaku® MiniFlex benchtop XRD instrument. To control the hydration state of the material an Anton Paar BTS500 heating stage attachment is used. The BTS500 operates from room temperature to 500 °C. The sample holder material is Nickel. The humidity is controlled with a similar home-built humidifier where a wet gas (air at 100% RH) at 18 °C and a dry gas (air at 0% RH) are mixed (resulting in a water vapour pressure in between 0–20 mbar).

From the diffraction patterns, the crystallite size can be determined from the peak broadening using the Scherrer equation, using a general shape factor as determined by Scherrer [24]) and a wavelength of 0.154 nm for a copper anode tube.

2.6. SEM

The morphology of the samples is studied using scanning electron microscopy (SEM), for surface analysis use is made of a FEI Quanta 600 FEG field emission scanning electron microscope. Images are generated at high vacuum with an acceleration voltage of 2 kV. For elemental analysis a JEOL JSM-IT100 scanning electron microscope is used with energy dispersive spectroscopy (EDS) for elemental analysis of the doped materials. The analysis is performed at high vacuum with an acceleration voltage of 12 kV.

After crystallization the powder is post-dried in an oven at 130 °C, after this, the samples are stored and transported in an airtight flask to

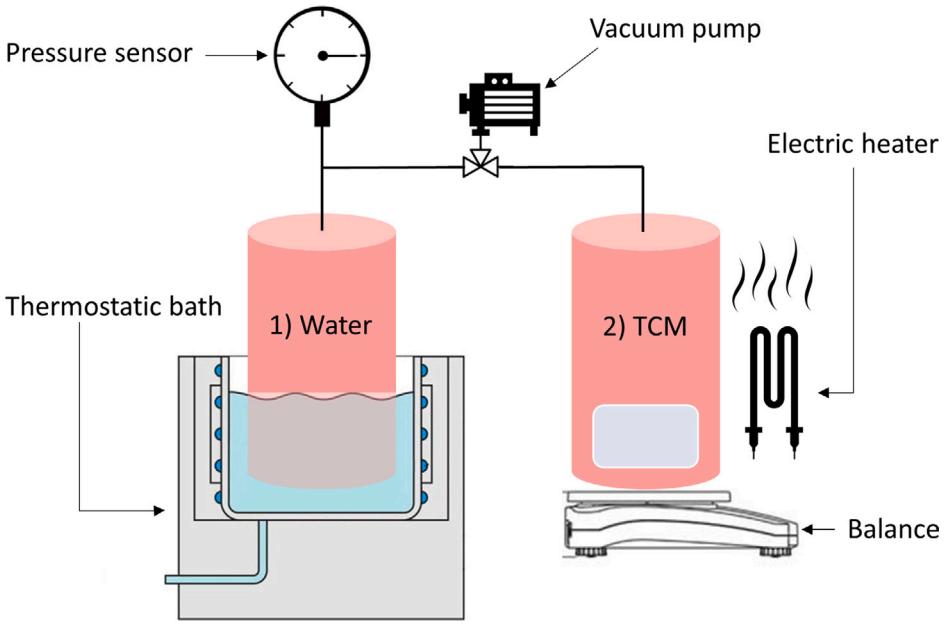

Fig. 2. Schematic illustration of the pT-mass setup. Vessel 1 contains water and acts as the evaporator/condenser, vessel 2 contains the TCM. The mass of vessel 2 is measured so the hydration state and kinetics can be measured. The system operated under pure water vapour conditions (vacuum). Both vessels are temperature controlled and the entire setup is heated to avoid internal condensation in the tubing.

prevent hydration during storage and transport. The powder (50–160 μm) is attached on 12.55 mm aluminum stubs using double sided carbon tape. The sample preparation is done under ambient condition but the open-time is minimized (t<30 s).

2.7. Multi-cyclic stability

To assess the multi-cyclic stability, 1 g of material is cycled in a small scale reactor setup. After cycling a single hydration curve is measured in the TGA. The small scale reactor is shown in Fig. 2, where the mass of vessel 2 is measured over time. The system works in vacuum, thus the material is cycled under pure water vapour conditions. Vessel 1 contains liquid water and is temperature controlled and thus acts as evaporator/condenser, vessel 2 contains the TCM and is also temperature controlled. For this study the setup will be used only for material cycling. A detailed description of the setup can be found in [11]

3. Results

3.1. Crystallographic data of doped K_2CO_3

In these experiments the diffraction patterns of all doped samples are compared to those of pure K_2CO_3 to determine if the crystal structure of pure K_2CO_3 is affected. All samples were pre-dried at 130 °C (t > 24 h) and the measurement are performed at 120 °C, to secure all diffraction patterns are of anhydrous samples. Fig. 3(a) shows the diffraction patterns of the pure and doped samples i.e. from bottom to top Li_2CO_3-, Na_2CO_3-, pure, Rb_2CO_3- and Cs_2CO_3-doped K_2CO_3 respectively. The *Y*-axis indicates the relative intensity of each sample with respect to its highest intensity.

All diffraction patterns correspond to the diffraction pattern of pure K_2CO_3 except for Na_2CO_3-doped K_2CO_3. For the Na_2CO_3 doped samples, some peaks correspond to those of pure K_2CO_3 but new peaks with high relative intensities appear (29, 33 and 35°). Apart from Na_2CO_3, the other dopants do not influence the crystal lattice of the dominant crystalline phase (K_2CO_3). It is therefore assumed that except from Na_2CO_3 the other dopants are not built-in to the crystal lattice of K_2CO_3, but decorate the surface of K_2CO_3. The intensity of the minor peaks of the dopant is very limited.

To understand the Na_2CO_3 doped sample, Fig. 3(b) shows the peaks at 29 and 33° in more detail of the system Na_2CO_3-K_2CO_3. It can be seen that the diffraction pattern of the doped sample does not correspond to one of both base constituents (K_2CO_3 or Na_2CO_3), this indicates that a co-crystal has been formed consisting of both Na_2CO_3 and K_2CO_3. Furthermore, the diffraction pattern is also compared with crystallographic data (CIF) from literature of the hydrated state; $K_2CO_3 \cdot 1.5\ H_2O$ [25]. From this it is concluded that the peaks of the Na_2CO_3-K_2CO_3 sample do not correspond to the hydrate of K_2CO_3 (data not shown here), underlying that a co-crystal of both Na_2CO_3 and K_2CO_3 has been formed .

3.2. Primary crystallite size

Next to crystal structural analysis, XRD can also be used to determine the coherent scattering domain size, which is a measure for the primary crystal size. In a poly-crystalline material a grain consists of several hundreds/thousands crystallites and a particle is composed of several grains. The crystallite size is important since the crystallite size can have an effect on the reaction kinetics. In this section we therefore compare the crystallite sizes of all the doped samples to pure material (K_2CO_3), where we are especially interested in the relative difference in between the sample. Using the peak broadening with the Scherrer equation, the coherent scattering domains can be determined, the result are shown in Fig. 4.

The crystallite size of all samples are quite similar. Therefore, potential significant kinetic effects cannot be caused by a differences in primary crystallite size.

3.3. Onset points for hydration, dehydration and deliquescence

In this section the results of the onset points, for hydration, dehydration and deliquescence are discussed as measured with TGA (isobaric at 17 mbar water vapour pressure). The five different markers indicate pure K_2CO_3, and Li_2CO_3-, Na_2CO_3-, Rb_2CO_3- and Cs_2CO_3-doped K_2CO_3.

First, it can be seen that all deliquescence points coincide with that of pure K_2CO_3, except for Cs_2CO_3. In presence of Cs_2CO_3 the deliquesce

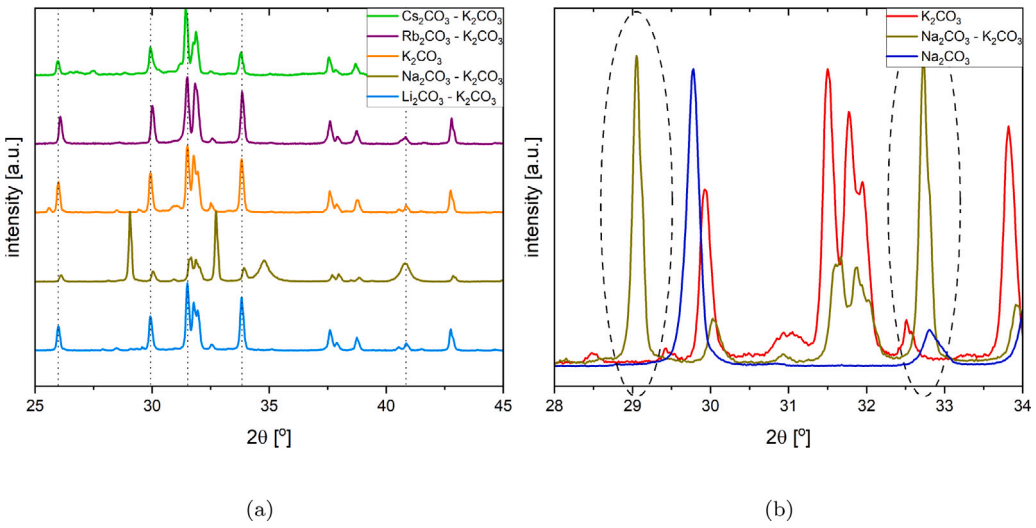

Fig. 3. (a). Diffraction patterns of all anhydrous doped- and pure K_2CO_3 (as prepared by crystallization, content; Li_2CO_3 2.2, Na_2CO_3 19.4, Rb_2CO_3 5, Cs_2CO_3 5 mol %). (b) Zoom in on the diffraction pattern of pure Na_2CO_3, K_2CO_3 and Na_2CO_3- doped K_2CO_3, indicating distinct peaks not corresponding to pure K_2CO_3.

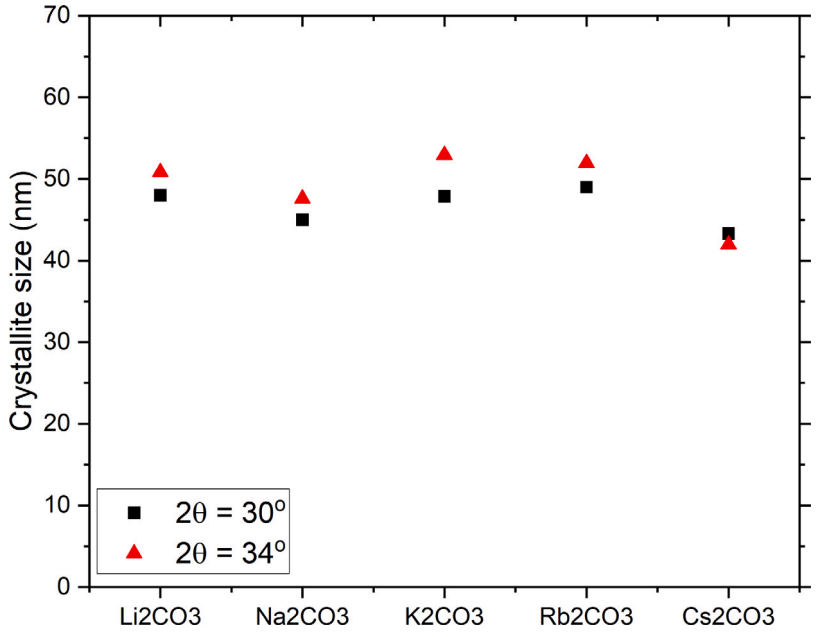

Fig. 4. Crystallite size of all doped samples, determined using the Scherrer equation at a 2Θ of 30 and 34°.

onset temperature shifts from 29 °C for pure K_2CO_3 to 36 °C. In terms of relative humidity, this is a shift from 43% to 29% RH.

Secondly, the onset points for hydration coincide with the hydration onset point of pure K_2CO_3 and is in agreement with Sögütoglu et al. [12], except for Cs-doped K_2CO_3. The shift in hydration onset point for Cs_2CO_3 doping is 3 K, reducing the metastable zone width (MZW) at 17 mbar from 10 K to 7 K, i.e. a reduction of the MZW for hydration of 30%.

Thirdly, the dehydration onset points are somewhat more spread, but still close to pure K_2CO_3. Again Cs-doped K_2CO_3 is the exception. Due to caesium the onset point shifts for 5 K, reducing the MZW from 12 K to 7 K for dehydration, resulting in a reduction of the MZW for dehydration of 42%.

To analyse if the effect is caused by the preparation method or the doping intrinsically, three different preparation methods are used; freeze drying, melting and forced crystallization. Fig. 5(b) shows the results. It can be seen that the hydration and dehydration match very accurately, a minor spread is found in the deliquescence onset points but they still match very good. It can thus be concluded that the effect of caesium doping is independent of the preparation method and the effect is thus intrinsically due to the dopant.

3.4. *Metastable zone lines Cs_2CO_3-doped K_2CO_3*

As only Cs_2CO_3 significantly reduces the MZW at 17 mbar, the full metastable zone boundaries of Cs_2CO_3 doped K_2CO_3 have been determined, see Fig. 6.

The triangles indicate the onset points for hydration, whereas the squares indicate the onset points for dehydration. These measurements show a reduction of the meta-stable zone for both hydration and dehydration over a wide range of vapour pressures from 6–18 mbar. Overall the shift in onset point is the largest for dehydration. Due to

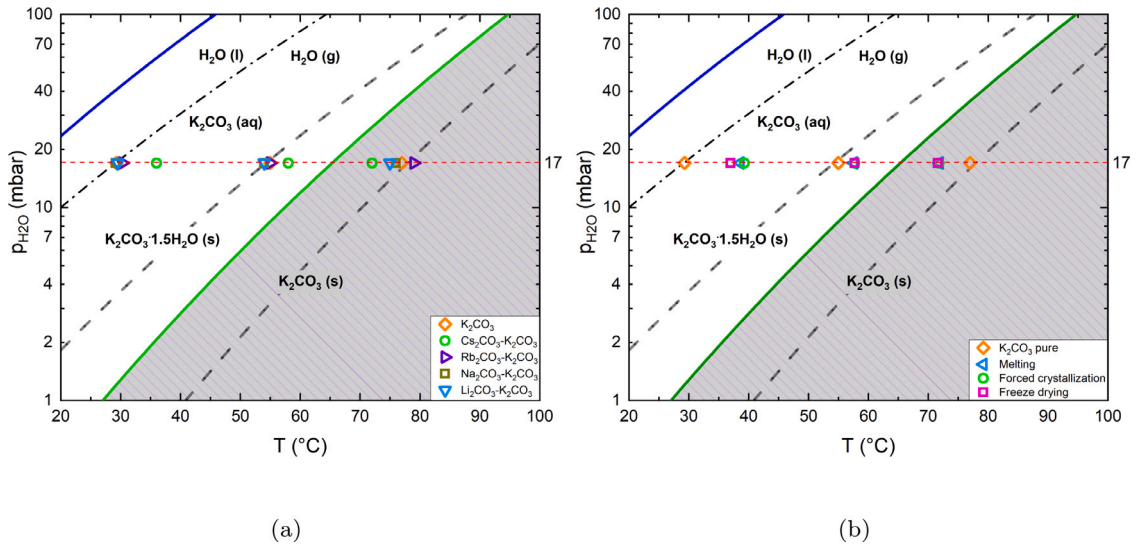

Fig. 5. (a) Onset point screening for all dopants at a isobaric water vapour pressure of 17 mbar (as prepared by crystallization, content; Li_2CO_3 2.2, Na_2CO_3 19.4, Rb_2CO_3 5, Cs_2CO_3 5 mol %). From left to right the deliquescence, hydration and dehydration onset points. (b) Screening for caesium doping prepared with three different methods; crystallization, melt and freeze drying (content for all methods 5 mol %).

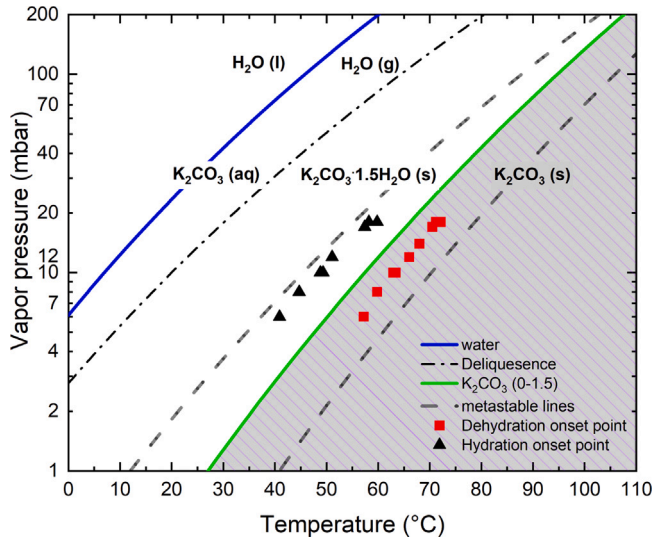

Fig. 6. Metastable zone width screening of Cs_2CO_3-doped K_2CO_3 over a range of vapour pressures from 6–18 mbar. The green solid line is the equilibrium line, the dashed lines are the metastable lines and the dashed–dotted line is the deliquescence line. The blue solid line is the water line.

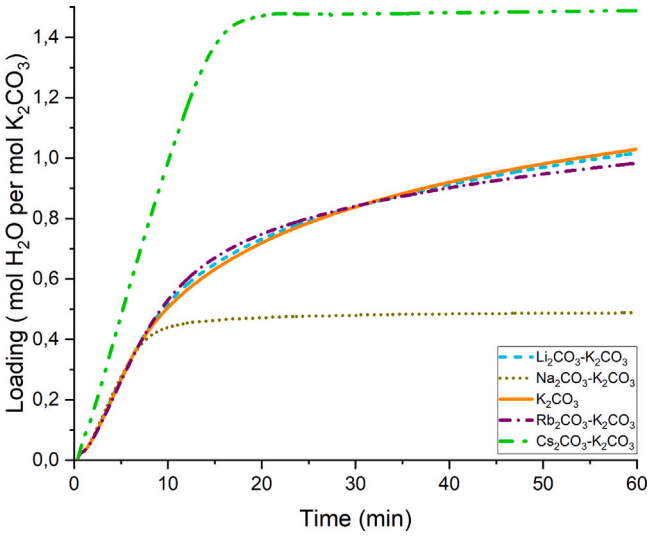

Fig. 7. Hydration of pure and Li_2CO_3, Na_2CO_3, Rb_2CO_3 and Cs_2CO_3- doped K_2CO_3, performed at p_w = 12 mbar and T = 40 °C (as prepared by crystallization, content; Li_2CO_3 2.2, Na_2CO_3 19.4, Rb_2CO_3 5, Cs_2CO_3 5 mol %).

this shift in hydration and dehydration onset points the temperature operating window of K_2CO_3 is significantly improved by doping with Cs_2CO_3.

3.5. Reaction kinetics

The other objective of doping is to improve the kinetics outside the metastable zone. Therefore, a kinetic screening is performed at isothermal and isobaric conditions (p_w = 12 mbar and T = 40 °C). The temperature of the material is stabilized before the water vapour pressure is supplied. Fig. 7 show the results, with the loading i.e. mol water per mol K_2CO_3, on the Y-axis and the time on the X-axis.

It can be seen that the Li_2CO_3 and Rb_2CO_3 doping have no effect on the hydration rate of K_2CO_3. Both Na_2CO_3 (dark yellow) and Cs_2CO_3 (green) do have an effect on the hydration rate of K_2CO_3. In presence of Na_2CO_3 the initial hydration rate is similar to that of pure K_2CO_3, however, the final loading is below 0.5 H_2O/mol K_2CO_3, indicating that part of the material does not bind water which can be understood since a part of the material has formed a co-crystal which does not absorbs water (at least under the current conditions).

Cs_2CO_3 doping significant accelerates the kinetics. Firstly, the end conversion is reached within 20 min, whereas for pure K_2CO_3 the loading has only reached 1.0 mol H_2O/mol K_2CO_3 after 60 min. Secondly, the hydration rate is almost linear over the full conversion.

This becomes even clearer when the hydration rate is shown as function of the conversion, this is shown in Fig. 8.

What can be observed here is that hydration mechanisms are significantly different. Sögütoglu et al. [26] has shown that for pure K_2CO_3, the reaction rate is limited by diffusion of water towards the reacting surface when conversion progresses. For Cs_2CO_3 this is significantly different, the initial conversion seems to be limited by nucleation and growth, but after 15% conversion the reaction kinetics does not rapidly decrease. Based on the work of Khawam and Flanagan [27], the

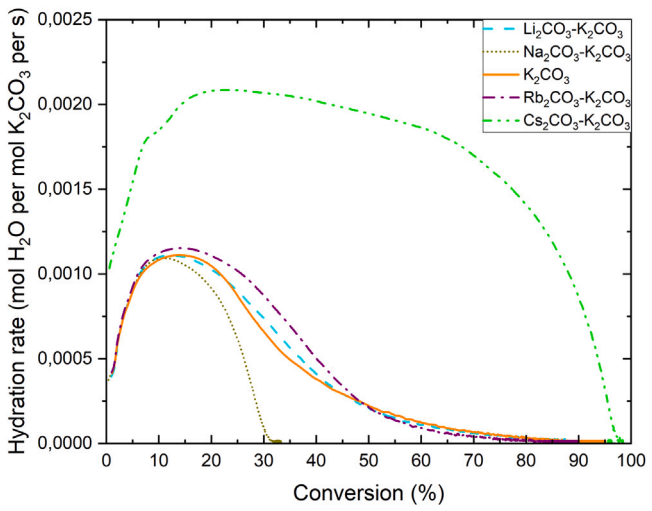

Fig. 8. The hydration rate as function of conversion for all doped samples and pure K_2CO_3.

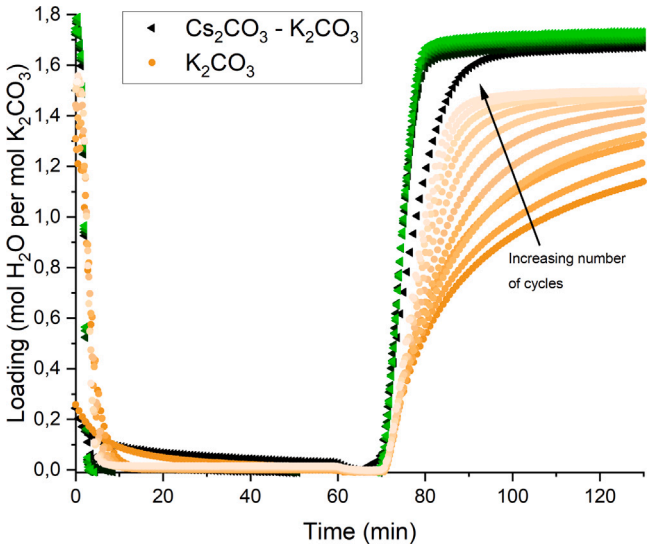

Fig. 9. Cyclic TGA of pure K_2CO_3 and Cs_2CO_3-doped K_2CO_3. The experiment is done under isobaric conditions (p_w = 12 mbar) and thermal cycling between 140 and 40 °C. With increasing cycle the line colour becomes lighter; dark orange to light orange for pure K_2CO_3 and from dark green/black to light green.

reaction of caesium doped K_2CO_3 is in the class of the geometrical contraction (R) models which indicates that the reaction rate is dominated by the reacting interface.

3.6. Cyclic behaviour

Cyclic behaviour of Cs-doped K_2CO_3 is explored in 10 sequential hydration–dehydration cycles using TGA. Doped and undoped K_2CO_3 is compared. The experiments are performed at a constant water vapour pressure of 12 mbar and the temperature is cycled between 140 and 40 °C. Fig. 9 shows the results.

Obviously, the kinetics of pure K_2CO_3 increases during cycling. This cycling effect is due to an increase in internal surface area due to porosity build-up [28]. For Cs_2CO_3 the kinetics is already much faster

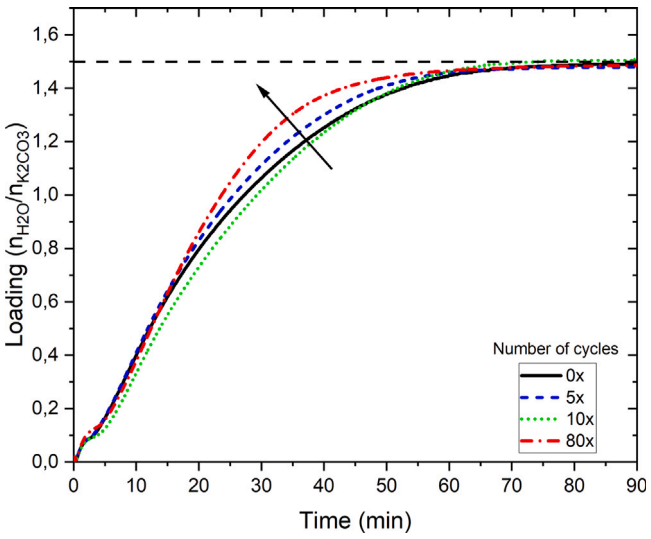

Fig. 10. Single hydration experiment of Cs_2CO_3-doped K_2CO_3, pre-cycled (0,10, 40 and 50 times) in a small scale reactor. Showing loading (Y-axis) versus time (X-axis). The experiment is performed at p_w 12 mbar and 40 °C.

from the start on and only takes 1 cycle to become stable. Moreover, the overall kinetics is faster for the doped sample, being stable over 10 cycles.

To verify the cyclic stability over more cycles the doped material has been cycled 80 times in a small scale reactor as described in Section 2.7. During cycling part of the material is extracted from the reactor setup and a single hydration experiment is performed. Fig. 10 shows the result.

It is shown that the hydration rate is relatively stable for all cycles between 0 and 80 cycles. This indicates that the effect caused by the dopant is stable during cycling, no re-crystallization in separate phases seems to occurs between $K_2CO_3$and Cs_2CO_3. Thereby we conclude that the location of the dopant does not change during cycling.

3.7. SEM

In the previous section it is shown that the dopant is stable during cycling, but the precise location of the dopant is still unknown. To investigated where the dopant is located, SEM-edx used. Fig. 11 shows a SEM image of pure K_2CO_3 and 5% Cs_2CO_3 doped K_2CO_3, depicting a surface structure of the caesium doped sample that is less well-defined.

Small surface structures seem to overlap with larger structures on the grain, as indicated with the circles in Fig. 11(b). Overall, it seems that the small grains on the surface are more agglomerated with the larger grain. On the pure K_2CO_3 sample, a large grain can be identified on which smaller grains are not agglomerated (indicated with the circle in Fig. 11(a)). If the dopant (in Fig. 11(b)) attracts more water on the surface, more agglomeration can be expected. In the work of Dupas-Langlet et al. [29], where the impact of deliquescence lowering on powders has been studied, an increase in water uptake on mixtures is observed and thereby a loss of crystallinity. Similar as in this work, SEM shows that caking leads to the formation of non-crystalline shaped agglomerates. On the pure K_2CO_3 sample in Fig. 11(a), these crystalline features can be identified and are indicated with the red arrows.

To get more detailed information on the surface composition, EDX is used with elemental mapping. Fig. 12 shows the results of a sample with 10% caesium doping. In the top, an overlay is shown of all elements; where green corresponds to potassium, red to caesium and blue to carbon. The bright blue carbon clusters are due to the carbon tape background. Qualitatively, there is no clear localization of clusters

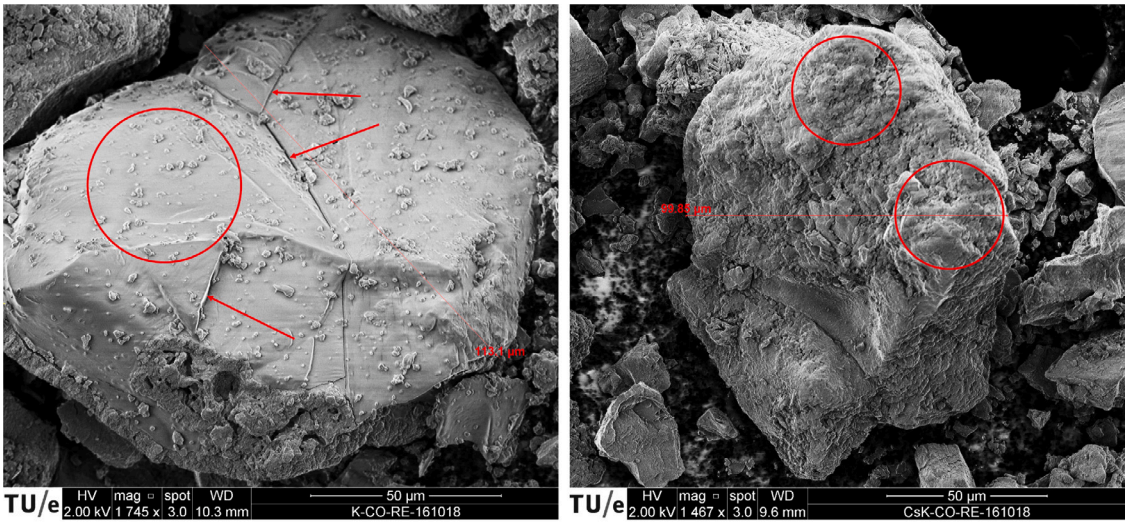

(a) (b)

Fig. 11. SEM images of pure and Cs_2CO_3 doped K_2CO_3. (a) Pure K_2CO_3, a large grain with on the surfaces smaller crystallites at which crystal habits can be recognized (red arrows). (b) Cs_2CO_3-doped K_2CO_3, on the surfaces the structures seem to be agglomerated, no individual crystal habits can be recognized.

of caesium on the surface of the grains. It is therefore assumed that the doping is homogeneously distributed over the surface.

In summary, two observations are made; firstly, the crystal surface seems to be more agglomerated in which no crystal habits are recognized and secondly, no local clusters of caesium are found indicating that the dopant is uniformly distributed.

3.8. Hydration mechanism by caesium doping

Caesium doping affects the onset points of the phase transition of potassium carbonate. Moreover, a significant kinetic acceleration of kinetics is observed with the addition of caesium doping. To understand how caesium affects the phase transition of K_2CO_3, the content of Cs_2CO_3 is varied.

Fig. 13 shows results of an isobaric experiment with changing temperature. An onset measurement is performed as described in Section 2.4. The experiment starts at 140 °C (with constant water vapour pressure of 17 mbar) until the sample is completely dehydrated, after which the temperature is reduced with a cooling rate of 1 K/min until 40 °C, where the sample is fully hydrated, followed by heating until dehydration starts. On the right Y-axis the temperature is shown, which corresponds to the red line and on the left Y-axis the loading is displayed and corresponds to all other curves, on the X-axis the time is plotted.

Four features are of special interest; (1) the end loading (at T = 40 °C) increases with increasing caesium content, (2) water is released instantaneously when the temperature is increased (at 5.7 h) and (3) after initial water release a second transition is observed and (4) water is already absorbed before hydration starts.

First the effect indicated with (1) shows that the end loading increases with an increasing amount of Cs-doping. The effect indicated with (2) shows that when the temperature is increased, water desorbs instantaneously. This indicates that this water is mobile, as only mobile water can evaporate instantaneously. Crystal water will be released at a well defined dehydration temperature. At (3) a second transition is observed, here bulk dehydration of K_2CO_3 takes place.

Fig. 14 zooms in on effect 4 by plotting the loading as function of temperature. Only the data shown is for t < 5.5 h.

At the start of the experiment, the material is prepared fully anhydrous (loading is zero). The orange curve corresponds to pure K_2CO_3, hydration starts at 55 °C which corresponds to the metastable zone, as found by Sögütoglu et al. [12]. With increasing amounts of caesium doping, the hydration of bulk K_2CO_3 starts at a higher temperature. Moreover, in the presence of dopants water is absorbed at a significant higher temperature (before 85 and 95 °C) for the doped material, there is water uptake. The effects 1, 2 and 4 all indicate that a fraction of the absorbed water is attracted by Cs_2CO_3 to the surface and is present in a disordered state. Presumably this disordered state is far more mobile then the K_2CO_3 crystal itself.

To have a better view on how this mobility is introduced, the same experiment for pure Cs_2CO_3 is performed, the result is shown in Fig. 15.

A heating/cooling rate of 1 K/min is used and a water vapour pressure of 17 mbar. There is already water uptake at a temperature of 98 °C. This initial uptake indicates hydrate formation as the loading converges to an equilibrium. At 87 and 73 °C, a second and third hydration transition are observed respectively. Then at 56 °C, the sample goes into deliquescence, as the water uptake increases without converging to equilibrium. The dashed line indicates the temperature where pure K_2CO_3 starts to hydrate, this is very close to the point where Cs_2CO_3 goes into deliquescence. During dehydration the temperature is increased, however, the sample does not seem the recrystallize and stays in a deliquescence condition. If we link this to effect 4) observed in Fig. 13, where there is mobility observed, this can be explained by the current observation of the behaviour of pure Cs_2CO_3, where there is a metastable deliquescence state which introduces this mobility.

4. Discussion

It is shown that caesium doping significantly affects the hydration rate and temperature operating window of K_2CO_3. In this section the results of the different sections are combined to postulate how the caesium doping enhances the performance of K_2CO_3. Cs_2CO_3 did not influence the crystal lattice of K_2CO_3. It is therefore concluded that caesium is not built into the crystal lattice of K_2CO_3, but decorates the surface of K_2CO_3. Furthermore from the crystallite size analyses it is shown that of all samples the crystallite sizes are the same. Therefore, kinetic effects due to Cs_2CO_3 cannot be caused by the primary

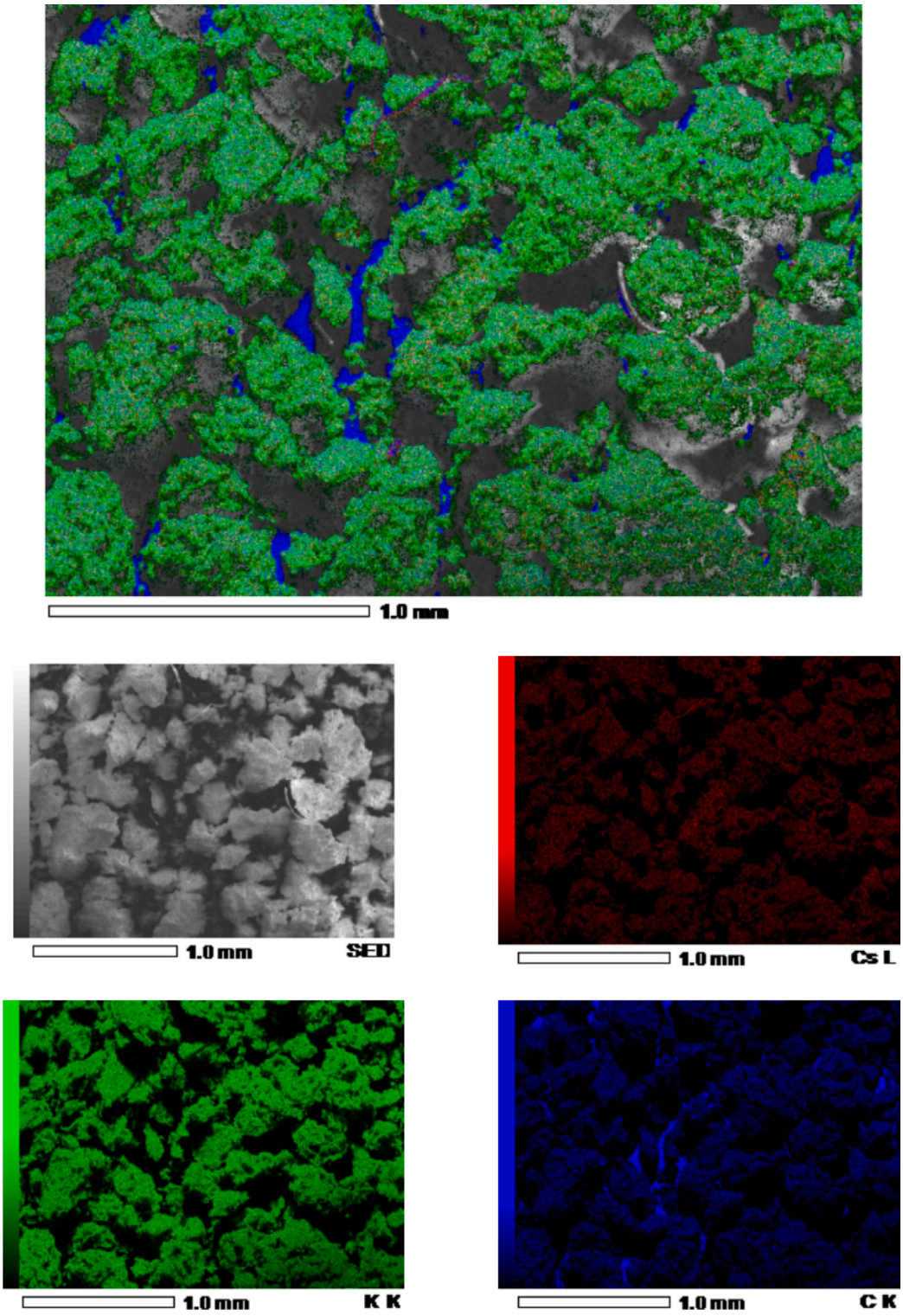

Fig. 12. SEM EDX with elemental mapping of a 10% ceasium doped sample. In the top an overlay of all colours representing the different elements is shown. In the lower graphs a mapping of; in red caesium (Cs), in green potassium (K) and in blue carbon (C) elements.

crystallite size. That caesium doping; narrows the meta-stable zone and increases the hydration kinetics, should be due to the caesium dopant on the surfaces of K_2CO_3 crystals.

It has been shown in Section 3.5, that the hydration mechanism for the caesium doped sample is significantly different. Sögütoglu et al. [26] has shown that for pure K_2CO_3, the reaction rate is limited by diffusion of water but in this work it is shown that for Cs_2CO_3 the reaction rate of caesium doped K_2CO_3 is dominated by the reacting interface.

Combining this reaction model with the observations that surface mobility is introduced due to increased water absorption on the surface by the presence of Cs_2CO_3 (Section 3.8), we conclude that the increased

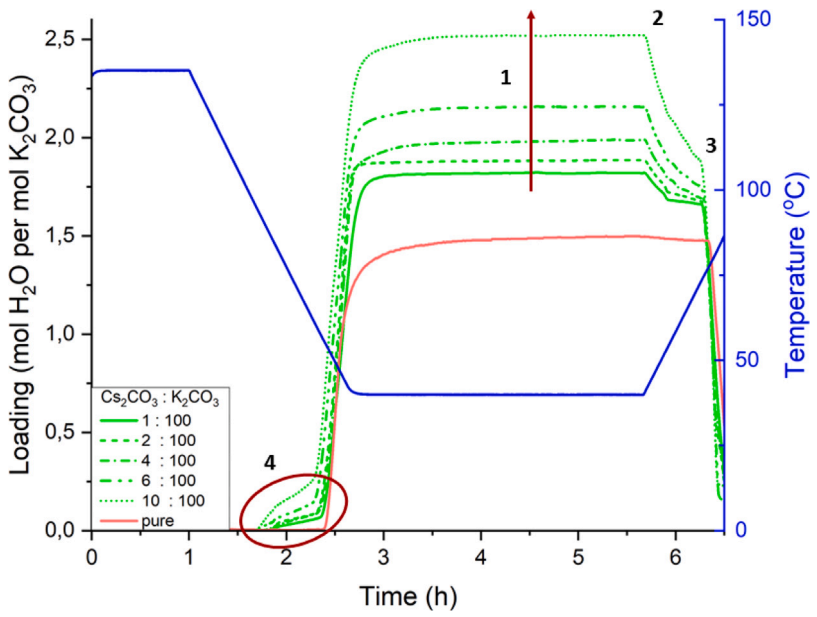

Fig. 13. Isobaric measurements on sample with different Cs_2CO_3 content. On the left *Y*-axis the loading is shown and corresponds to all other curves, on the *X*-axis time is plotted. The right axis corresponds to the blue line and indicates the sample temperature. The orange line is pure K_2CO_3 and the green lines are different amounts of doping. The doping content varies from 1:100–10:100 (mol:mol).

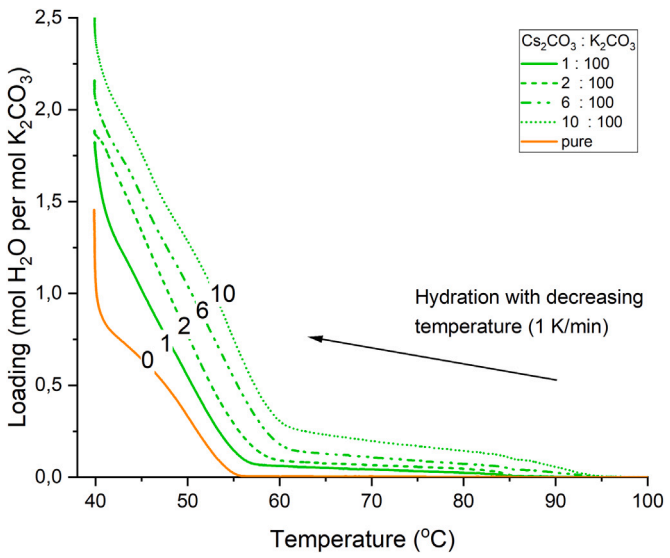

Fig. 14. Loading during hydration at fixed water vapour pressure (17 mbar). With respect to time the curve should be read from high to low temperature, so the start is at loading zero. The water vapour pressure is 17 mbar. Two onset points are observed, initial water adsorption by caesium (between 85–95 °C) and bulk hydration of K_2CO_3 above 55 °C.

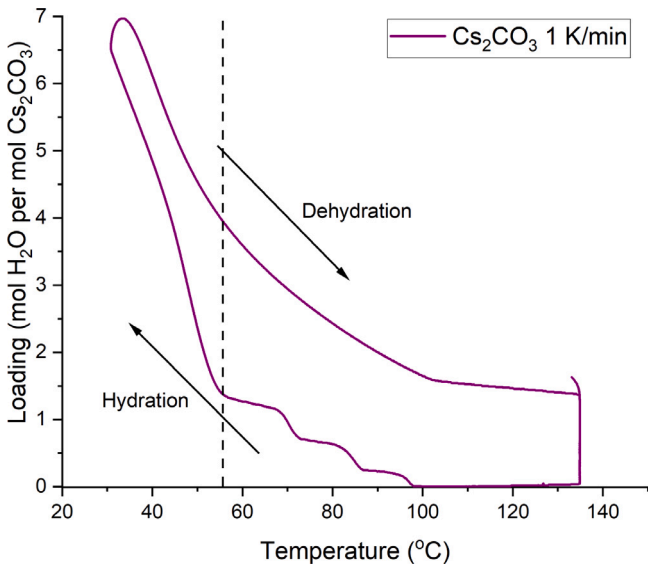

Fig. 15. Isobaric TGA run of pure Cs_2CO_3 at 17 mbar water vapour pressure. The dashed line indicates the hydration onset point of pure K_2CO_3.

surface mobility changes the reaction mechanism from a diffusion limited reaction towards a reacting interface mechanism. Whereby the increased water absorption is due to the fact that Cs_2CO_3 goes into deliquescence at lower DRH, contributing to an increased mobility at the surface, which is a prerequisite for the phase transition [14].

5. Conclusion

In this work several doping candidates for K_2CO_3 are selected, prepared and screened. The onset point screening at isobaric conditions showed that only Cs_2CO_3 affects the onset points; for hydration, dehydration and deliquescence of K_2CO_3. This results in a significant reduction of the metastable zone width; 30% for hydration and 42% for dehydration. Therefore, a significant increase in the temperature operating window is achieved with caesium doping. However the DRH is also shifted, from 43 till 29%. This increases the risk of deliquescence.

A kinetic screening shows that only caesium increases the hydration rate of K_2CO_3. Additionally, with caesium doping, the peak hydration rate is being more then a factor of two higher and the hydration rate is almost constant over the whole conversion. Furthermore, the change in conversion behaviour indicates that the hydration mechanisms are significantly different, for K_2CO_3 the behaviour is more diffusion limited when conversion increases, while for Cs_2CO_3 this is not the case and the reaction kinetics itself is limiting [26]. The constant reaction

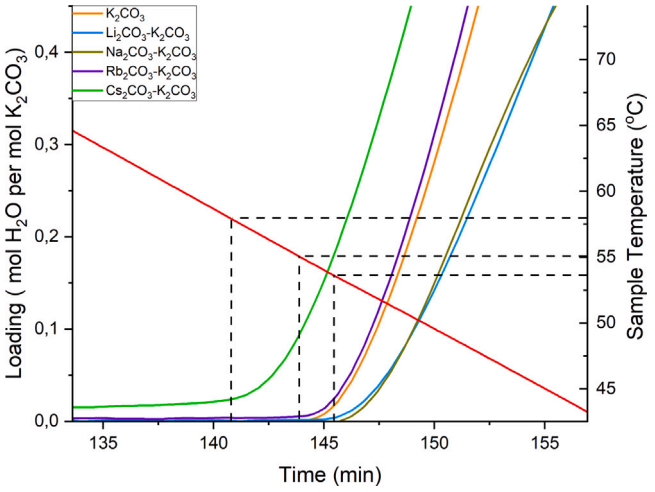

Fig. A.16. Onset point screening; isobaric (17 mbar) TGA run of Li_2CO_3-, Na_2CO_3-, Rb_2CO_3-, Cs_2CO_3-doped and pure K_2CO_3, temperature is reduced at 1 K/min. The onset point is determined as the point where the initial water uptake takes place (deviation from the base line).

rate is extremely crucial for heat battery applications as this results in a more constant power output.

With XRD it has been shown that the caesium doping is not built into the crystal lattice of K_2CO_3, and is thus present on the surface of K_2CO_3. SEM has shown that the crystal surface seems to be more agglomerated and that there are no local clusters of caesium. This indicates that the dopant is homogeneously distributed over the surface.

Finally, the reduction of the metastable zone and acceleration of kinetics seems to be caused by the formation of a mobile layer due to the caesium. Caesium doping facilitates the formation of a mobile layer by attracting water at the crystal surface and thereby enhancing the hydration reaction. The formation of this mobile layer is correlated with the lower DRH of caesium carbonate. That the hydration transition is promoted by a dopant which enhances mobility, matches very well with the conclusion made by Sögütoglu et al. [12], that the solid–solid phase transition is mediated by a mobile wetting layer. Caesium doping thus facilitates this wetting layer.

This work thus shows that the performance of K_2CO_3 can be improved by caesium doping. As such this study provides the insights for a more targeted development of high power salt hydrate based TCM materials.

CRediT authorship contribution statement

Jelle Houben: Writing – review & editing, Writing – original draft, Visualization, Methodology, Investigation, Formal analysis, Data curation, Conceptualization. **Aleksandr Shkatulov:** Writing – review & editing, Conceptualization. **Henk Huinink:** Writing – review & editing, Supervision, Methodology, Conceptualization. **Hartmut Fischer:** Writing – review & editing, Supervision, Methodology, Conceptualization. **Olaf Adan:** Writing – review & editing, Validation, Supervision, Resources, Funding acquisition, Conceptualization.

Declaration of competing interest

The authors declare that they have no known competing financial interests or personal relationships that could have appeared to influence the work reported in this paper.

Data availability

Data will be made available on request.

Acknowledgements

This work was funded by the TKI project Dope4Heat with project number 1507201 and the Dutch Organization for Applied Research (TNO). This work reflects only the authors view. The authors thank Hans Dalderop and Jef Noijen for their technical support.

Appendix

The original TGA curves from which the onset points in Fig. 5(a) are determined are shown in Fig. A.16. The measurements are performed at a constant water vapour pressure of 17 mbar, while the temperature is lowered at a rate of 1 K/min.

The onset points are determined from the point where the initial water absorption takes place, the point where the loading increases. The baseline of the Cs_2CO_3 doping is higher since the initial water uptake by the dopant starts at a temperature > 90 °C.

References

[1] European Commission, Roadmap 2050, Policy (April) (2012) 1–9, http://dx.doi.org/10.2833/10759, URL http://www.roadmap2050.eu/, arXiv:ISBN978-92-79-21798-2.

[2] S. Hallegatte, J. Rogelj, M. Allen, L. Clarke, O. Edenhofer, C.B. Field, P. Friedlingstein, L. van Kesteren, R. Knutti, K.J. Mach, M. Mastrandrea, A. Michel, J. Minx, M. Oppenheimer, G.-K. Plattner, K. Riahi, M. Schaeffer, T.F. Stocker, D.P. van Vuuren, Mapping the Climate Change Challenge, Vol. 6, Nature Publishing Group, 2016, http://dx.doi.org/10.1038/NCLIMATE3057, URL www.nature.com/natureclimatechange.

[3] K. Edem N'tsoukpoe, T. Schmidt, H.U. Rammelberg, B.A. Watts, W.K.L. Ruck, A systematic multi-step screening of numerous salt hydrates for low temperature thermochemical energy storage, 2014, http://dx.doi.org/10.1016/j.apenergy.2014.02.053.

[4] A. Fopah Lele, K.E. N'Tsoukpoe, T. Osterland, F. Kuznik, W.K. Ruck, Thermal conductivity measurement of thermochemical storage materials, Appl. Therm. Eng. 89 (2015) 916–926, http://dx.doi.org/10.1016/j.applthermaleng.2015.06.077.

[5] T. Kousksou, P. Bruel, A. Jamil, T. El Rhafiki, Y. Zeraouli, Energy storage: Applications and challenges, Solar Energy Mater. Sol. Cells 120 (PART A) (2014) 59–80, http://dx.doi.org/10.1016/j.solmat.2013.08.015.

[6] P.A. Donkers, L.C. Sögütoglu, H.P. Huinink, H.R. Fischer, O.C. Adan, A review of salt hydrates for seasonal heat storage in domestic applications, Appl. Energy 199 (2017) 45–68, http://dx.doi.org/10.1016/j.apenergy.2017.04.080.

[7] L. Glasser, Thermodynamics of inorganic hydration and of humidity control, with an extensive database of salt hydrate pairs, J. Chem. Eng. Data 59 (2) (2014) 526–530, http://dx.doi.org/10.1021/je401077x, URL http://pubs.acs.org/doi/abs/10.1021/je401077x.

[8] L. Glasser, H. Donald, B. Jenkins, The thermodynamic solvate difference rule: Solvation parameters and their use in interpretation of the role of bound solvent in condensed-phase solvates, 2007, http://dx.doi.org/10.1021/ic701105p, URL https://pubs.acs.org/sharingguidelines.

[9] R.D. Boer, Determination of structural, thermodynamic and phase properties in the Na_2S – H_2O System .... No. May 2017, 2002, pp. 2–19.

[10] R.W. Carling, Dissociation pressures and enthalpies of reaction in $MgCl_2 \cdot nH_2O$ and $CaCl_2 \cdot nNH_3$, J. Chem. Thermodyn. 13 (6) (1981) 503–512, http://dx.doi.org/10.1016/0021-9614(81)90105-1.

[11] J. Houben, L. Sögütoglu, P. Donkers, H. Huinink, O. Adan, K_2CO_3 in closed heat storage systems, Renew. Energy 166 (2020) 35–44, http://dx.doi.org/10.1016/j.renene.2020.11.119.

[12] L.C. Sögütoglu, M. Steiger, J. Houben, D. Biemans, H.R. Fischer, P. Donkers, H. Huinink, O.C. Adan, Understanding the hydration process of salts: The impact of a nucleation barrier, Cryst. Growth Des. 19 (4) (2019) 2279–2288, http://dx.doi.org/10.1021/acs.cgd.8b01908.

[13] V.I. Kalikmanov, Nucleation Theory, in: Lecture Notes in Physics, vol. 860, 2013, pp. 1–331, http://dx.doi.org/10.1007/978-90-481-3643-8, arXiv:1211.6245.

[14] J. Houben, Understanding the hydration process of salts: The relation between surface mobility and metastability, 2021, Unpublished Manuscript.

[15] F. Höffler, I. Müller, M. Steiger, Thermodynamic properties of ZnSO4(aq) and phase equilibria in the ZnSO4–H2O system from 268 K to 373 K, J. Chem. Thermodyn. 116 (2018) 279–288, http://dx.doi.org/10.1016/j.jct.2017.09.012.

[16] M. Steiger, K. Linnow, H. Juling, S. Brüggerhoff, D. Kirchner, Hydration of $MgSO_4 \cdot H_2O$ and generation of stress in porous materials, Cryst. Growth Des. 8 (2008) 336.

[17] M. Steiger, S. Asmussen, Crystallization of sodium sulfate phases in porous materials: The phase diagram Na2SO4-H2O and the generation of stress, Geochim. Cosmochim. Acta 72 (17) (2008) 4291–4306, http://dx.doi.org/10.1016/j.gca.2008.05.053.

[18] H. Zondag, B. Kikkert, S. Smeding, R. de Boer, M. Bakker, Prototype thermochemical heat storage with open reactor system, Appl. Energy (2013) http://dx.doi.org/10.1016/j.apenergy.2013.01.082.

[19] L. Scapino, H.A. Zondag, J. Van Bael, J. Diriken, C.C. Rindt, Sorption heat storage for long-term low-temperature applications: A review on the advancements at material and prototype scale, Appl. Energy (2017) http://dx.doi.org/10.1016/j.apenergy.2016.12.148.

[20] A. Shkatulov, T. Krieger, V. Zaikovskii, Y. Chesalov, Y. Aristov, Doping magnesium hydroxide with sodium nitrate: A New approach to tune the dehydration reactivity of heat-storage materials, ACS Appl. Mater. Interfaces 6 (22) (2014) 19966–19977, http://dx.doi.org/10.1021/am505418z.

[21] A. Shkatulov, Y. Aristov, Modification of magnesium and calcium hydroxides with salts: An Efficient way to advanced materials for storage of middle-temperature heat, Energy 85 (2015) 667–676, http://dx.doi.org/10.1016/j.energy.2015.04.004.

[22] A. Shkatulov, Y. Aristov, Calcium hydroxide doped by KNO_3 as a promising candidate for thermochemical storage of solar heat, RSC Adv. 7 (68) (2017) 42929–42939, http://dx.doi.org/10.1039/c7ra06639b.

[23] L. Greenspan, Humidity Fixed Points of Binary Saturated Aqueous Solutions, Technical Report 1, Institute for Basic Standards, National Bureau of Standards, Washington, D. C., 1977, pp. 89–96.

[24] D.J. Lim, N.A. Marks, M.R. Rowles, Universal Scherrer equation for graphene fragments, Carbon 162 (2020) 475–480, http://dx.doi.org/10.1016/J.CARBON.2020.02.064.

[25] F.J. Skakle J. M. S, Wilson M., Dipotassium carbonate sesquihydrate: Rerefinement against new intensity data, 2001, pp. i94–i97.

[26] L.-C. Sögütoglu, F. Birkelbach, A. Werner, H. Fischer, H. Huinink, O. Adan, Hydration of salts as a two-step process: Water adsorption and hydrate formation, Thermochim. Acta 695 (October 2020) (2020) 178819, http://dx.doi.org/10.1016/j.tca.2020.178819.

[27] A. Khawam, D.R. Flanagan, Solid-state kinetic Models: Basics and mathematical fundamentals, J. Phys. Chem. B 110 (35) (2006) 17315–17328, http://dx.doi.org/10.1021/jp062746a.

[28] M.A. Beving, A.J. Frijns, C.C. Rindt, D.M. Smeulders, Effect of cycle-induced crack formation on the hydration behaviour of K_2CO_3 particles: Experiments and modelling, Thermochim. Acta 692 (2020) 178752, http://dx.doi.org/10.1016/j.tca.2020.178752.

[29] M. Dupas-Langlet, M. Benali, I. Pezron, K. Saleh, L. Metlas-Komunjer, The impact of deliquescence lowering on the caking of powder mixtures, Powder Technol. 270 (PB) (2015) 502–509, http://dx.doi.org/10.1016/J.POWTEC.2014.05.011.